minerals

MDPI

Article

Osteopontin and Vascular Endothelial Growth Factor-Immunoreactivity in Critical Bone Defects Matrix Production: A Nano-Hydroxyapatite/Beta-Tricalcium Phosphate and Xenogeneic Hydroxyapatite Comparison

Ivonete Sena dos Santos [1], Igor da Silva Brum [2,*], Victor Hugo Vieira de Oliveira [1], Ana Lucia Rosa Nascimento [1], Lucio Frigo [3], Mario José dos Santos Pereira [1] and Jorge José de Carvalho [1]

[1] Laboratory of Ultrastructure and Tissue Biology, Department of Histology and Embryology, State University of Rio de Janeiro, Rio de Janeiro 20550-900, Brazil; ivonetesena@gmail.com (I.S.d.S.); victorhvoabio@gmail.com (V.H.V.d.O.); ana.nascimento@uerj.br (A.L.R.N.); mariojps@gmail.com (M.J.d.S.P.); jjcarv@gmail.com (J.J.d.C.)
[2] Implantology Department, State University of Rio de Janeiro, Rio de Janeiro 20550-900, Brazil
[3] Periodontology Department, Universidade Guarulhos, Guarulhos 07023-070, Brazil; luciofrigo@uol.com.br
* Correspondence: Carvalho@uerj.br; Tel.: +55-21-988-244-976

check for updates

Citation: dos Santos, I.S.; da Silva Brum, I.; Vieira de Oliveira, V.H.; Rosa Nascimento, A.L.; Frigo, L.; dos Santos Pereira, M.J.; de Carvalho, J.J. Osteopontin and Vascular Endothelial Growth Factor-Immunoreactivity in Critical Bone Defects Matrix Production: A Nano-Hydroxyapatite/Beta-Tricalcium Phosphate and Xenogeneic Hydroxyapatite Comparison. *Minerals* **2021**, *11*, 1048. https://doi.org/10.3390/min11101048

Academic Editors: Josy A. Osajima, Edson Cavalcanti da Silva Filho, Maria Gardennia Fonseca and Denis Gebauer

Received: 2 September 2021
Accepted: 23 September 2021
Published: 27 September 2021

Publisher's Note: MDPI stays neutral with regard to jurisdictional claims in published maps and institutional affiliations.

Copyright: © 2021 by the authors. Licensee MDPI, Basel, Switzerland. This article is an open access article distributed under the terms and conditions of the Creative Commons Attribution (CC BY) license (https://creativecommons.org/licenses/by/4.0/).

Abstract: The development of new bone substitutes has become an area of great interest in materials science. In fact, hydroxyapatite is the most commonly used biomaterial in defects that require bone reconstruction, and that is certainly why the discovery of new products with its formulation has been increasing continuously. The aim of this study was to analyze the biological behavior of a xenogeneic hydroxyapatite widely disclosed in the literature and a synthetic nano-hydroxyapatite/Beta tricalcium phosphate in critical defects in the calvaria of Wistar rats. For this, the groups were divided as follows: 24 adult male Wistar rats were used, weighing between 300 and 350 g, in three groups with eight animals each. In the CTRL group (control), only the clot was kept, without material insertion; in the Bioss group (bovine hydroxyapatite), Bio Oss®—Gleistlich® was introduced; and in the Blue Bone group (REG), the defect was filled in with synthetic nano-hydroxyapatite associated with betatriphosphate of calcium, Blue Bone®—Regener®. According to the results in Goldner's Trichromics, we can observe a higher percentage of newly formed bone matrix in the REG group than in the CTRL and Bioss groups; in the VEGF, we had a more adequate cell modulation for blood vessel formation in the Blue Bone group (REG) compared to the Bioss and CTRL groups, while in osteopontin, a higher percentage of bone formation was observed in the Blue Bone group (REG) and Bioss group when compared to the CTRL group. We conclude that bone formation, mitosis-inducing cell modulation and main osteoblast activity were higher in the Blue Bone group (REG) than in the CTRL and Bioss groups.

Keywords: alloplastic; graft; nanohydroxyapatite; btcp

1. Introduction

Hydroxyapatite, an inorganic compound that constitutes 70% of the weight of bones and dental enamel, has been widely used for bone reconstruction surgeries [1], the development of new dental implant surfaces, and more recently in 3D technology for area replacement totally compromised by lesions caused by tumors or cancers of bone origin [2]. However, even though hydroxyapatite is already an established material in the literature, many studies seek to understand more deeply how the physicochemical behavior related to the cells involved in the ossification process occurs [3–5].

Recently, nanotechnology has been improving the bioactive properties of hydroxyapatite in relation to its crystals, resulting in a better response in association with nanocrystals

than with thicker crystals [6]. The crystallinity is the property responsible for the biomaterial remaining for more or less time in the body, and with these advances in the way the crystals are manufactured, it is possible to control not only the reabsorption time but also the replacement of the material more efficiently [7–9].

Another very important factor in the construction of a new biomaterial is its degree of porosity, which must be at a ratio greater than 50% [3]. This characteristic is directly correlated with better cell behavior, as it provides a more favorable environment for the proliferation and adequacy of cells involved in the ossification process, biomaterials with low porosity have a lower level of cellular response than biomaterials with more porosity, and consequently the production of extracellular matrix becomes irrelevant in relation to biomaterials with greater porosity [10].

The morphology of the particles must be considered when analyzing a new biomaterial; nanotechnology allows us to control the beginning, middle and end of the production of particles, and in this way it is possible to manufacture materials faithfully following what was predetermined at the beginning of the project. In addition, the standardization of particles provides a 30% to 50% increase in the surface area of the samples when related to micrometric materials [11]. These characteristics are directly correlated with the cells involved in the ossification process, especially in relation to osteoblasts, which, when compared to their activity as micrometric materials, was inferior in the formation of bone matrix compared to manometric materials [12].

The aim of this study was to compare the participation of osteoprogenitor cells and the extracellular matrix in the regeneration of critical bone defects with the application of grafts composed of nano-hydroxyapatite/Beta tricalcium phosphate of synthetic origin and hydroxyapatite of xenogeneic origin using histomorphometrics to compare the groups presented, generating a statistical result that would be relevant for a better analysis of the two biomaterials commonly used in guided bone regeneration surgeries.

2. Materials and Methods

2.1. Animals

The project was submitted to the Ethics Committee for the Care and Use of Experimental Animals, being approved by protocol 10/2020. Twenty-four adult male Wistar rats weighing between 300 and 350 g, produced by the vivarium of the Roberto Alcântara Gomes Biology Institute of the State University of Rio de Janeiro, were used. The animals were kept in cages with three animals from birth with access to food and water. A 12 h light/dark cycle and a temperature of 22 °C were both maintained throughout the project.

2.2. Surgical Procedures

The surgical procedures were performed in the laboratory of the Roberto Alcântara Gomes Biology Institute. Anesthesia was performed intraperitoneally, 1 mL for every 100 g of a combination of medications in 8.5 mL of 0.9% saline solution. The medications were: 0.2 mL of tramadol hydrochloride 5%, corresponding to 2 mg/kg, 0.5 mL of xylazine hydrochloride 2%, corresponding to 10 mg/kg, 1 mL of ketamine 10%, corresponding to 100 mg /kg, and 0.6 mL of midazolam maleate, corresponding to 5 mg/kg. When necessary, 1/3 of the solution was repeated after 20 min. After anesthesia of each specimen, the following surgical sequence was performed: trichotomy of the temporoparietal region with a No. 10 scalpel blade, antisepsis with povidine, triangular incision with a full-thickness flap with a 15 C scalpel blade, detachment of the skin and periosteum, and exposure of the surgical bone of the temporoparietal region with the Molt detacher, using an 8 millimeter diameter trephine (Alpha instruments SKU AI6005, SPSS v8.0 (IBM Corp., Armonk, NY, USA)) with a 20:1 counter-reducer angle (Driller do Brasil), coupled to the implant motor (Driller BLM 600), promotion of the critical bone defect from 8 millimeters to the dura mater (Figure 1), detachment of the trephined bone portion with a Molt spatula, replacement of the periosteum and skin, and suture of the flap with 3-0 nylon thread.

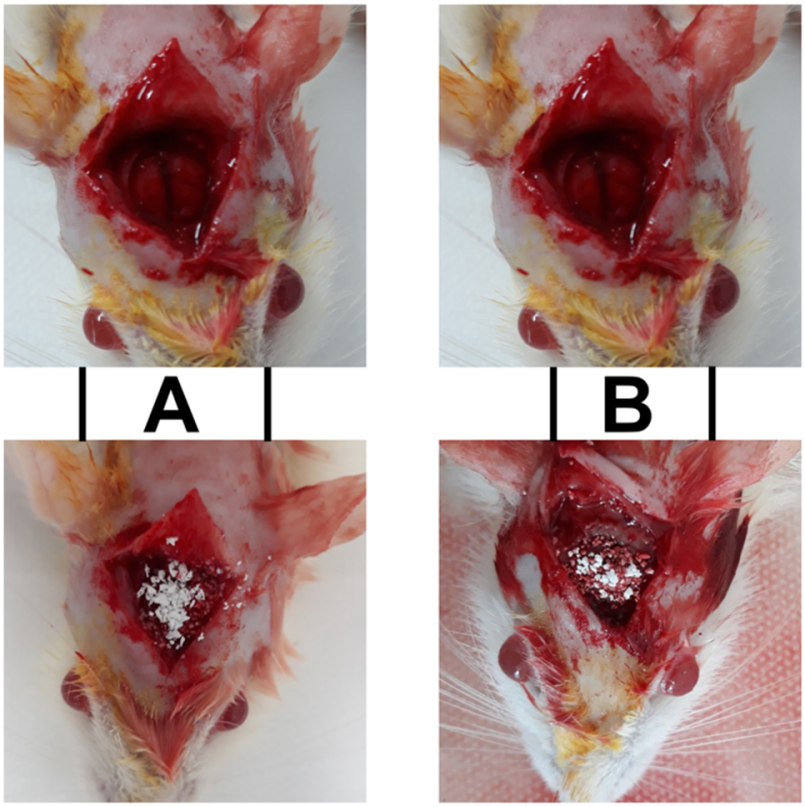

Figure 1. Photographs showing surgical procedures details: parietal bone osteotomy (8 mm diameter) to create the critical defect, followed by the biomaterial application: Bioss (**A**) and Blue Blone (**B**) groups.

2.3. Distribution of Groups

The animals were divided into 3 groups with 8 animals each. In the CTRL group (control), only the clot was kept, without material insertion, in the BO group (Bio Oss®, which does not have porous structure) [13], bovine hydroxyapatite (Geistlich, Wolhusen, Switzerland) was introduced, and in the other REG group, the defect was filled with nano-hydroxyapatite from Blue Bone® (porosity 63.84% and pore diameter size was from 0.10 to 18.08 μm) [3], synthetic origin (Regener, Curitiba, Brazil).

After 8 weeks of insertion of the materials in the bone defects, the animals were euthanized by anesthetic overdose. The animals' calvaria were separated for processing.

2.4. Morphological Analysis Protocol

The animals' calvaria were separated and fixed with paraformaldehyde for one week. Soon after, they were decalcified in EDTA (10%) in phosphate buffered saline (PBS) (0.1 M, pH 7.4) for 80 days. The samples were washed in distilled water and dehydrated alcohol (70%, 95%, 100%), clarified in dimethylbenzene and embedded in Paraplast™ (Sigma-Aldrich, St. Louis, MO, USA) at 65 °C. Serial 7 μm sections were cut into ceramic mass (LEICA, Nusslochonetos Siliceous, Wetzlar, Germany) and collected.

2.5. Goldner's Trichromic Staining Protocol

Weigert's hematoxylin was used for 10 min, washed in running water and rinsed in distilled water. Soon after, it was stained with Ponccau Acid Fuchsin dye for 5 min, washed with 1% acetic acid, inserted in phosphomolybdic acid-orange G solution until the collagen was discolored and washed in 1% acetic acid for 30 s. Then, the slide was stained in a light green solution for 5 min, washed in 1% acetic acid for 5 min and gently dried, just removing the excess. Then, the slide was quickly dipped in absolute alcohol,

dehydrated in 95% alcohol and absolute alcohol, with 3 passes each, and clarified in Xylene with 3 fluid changes.

2.6. Vascular Endothelial Growth Factor (VEGF) and Osteopomtin (OPN) Immunoreactivity

2.6.1. Histochemical Protocol

Histological slides were initially deparaffinized in xylol baths (3 × 5 min) and hydrated in decreasing concentrations of alcohol (100%, 90%, 70%) for 5 min in each bath. Slides were incubated in 3% hydrogen peroxide solution for 15 min in the dark, to inhibit endogenous peroxidase. After the inhibition of endogenous peroxidase activity, rinsing in PBS buffer at pH 7.2 was performed (3 × 5 min).

Antigenic site re-exposure was conducted in citrate buffer solution (pH 6.0 at 96 °C, for 20 min). After the slides cooled and were rinsed with a PBS buffer at pH 7.2 (3 × 5 min), nonspecific sites were blocked with PBS/BSA solution (3% for 20 min). After the rinsing, slides were incubated with the primary anti-VEGF antibody (Santa Cruz, sc-1876), diluted in PBS/BSA 1% (1:100) and primary anti-OPN antibody (Santa Cruz, sc-21742), and diluted in PBS/BSA 1% (1:200) overnight in a refrigerator (4.0 °C) in a humid chamber. After primary antibody incubation, 3 baths in PBS buffer solution at pH 7.2 (5 min) were carried out, followed by secondary biotinylated antibody (VECTASTAIN® Universal Quick HRP Kit, Ingold Road, Burlingame, CA, USA) incubation for 1 h at room temperature. After another PBS buffer solution rinse, slides were incubated with streptavidin (VECTASTAIN® Universal Quick HRP Kit) for 30 min at room temperature. The streptavidin–biotin–peroxidase complex was revealed with diaminobenzidine (DAB) (VECTASTAIN® Universal Quick HRP Kit). Slides were counterstained with hematoxylin solution (0.15%), dehydrated in increased alcohol concentrations (70%, 90%, 100%) (ethanol), diaphanized and mounted using Entellan resin (Sigma-Aldrich, St. Louis, MO, USA).

2.6.2. Image Acquisition and Histomorphometry

Goldner's trichrome-stained randomized slides were photographed with a photomicroscope (Carl Zeiss-JVC TK-1270 color video camera, Oberkochen, Germany) at 40× magnification. The images were quantified using GraphPad Prism version 8.0 (GraphPad, San Diego, CA, USA) (Figure 2).

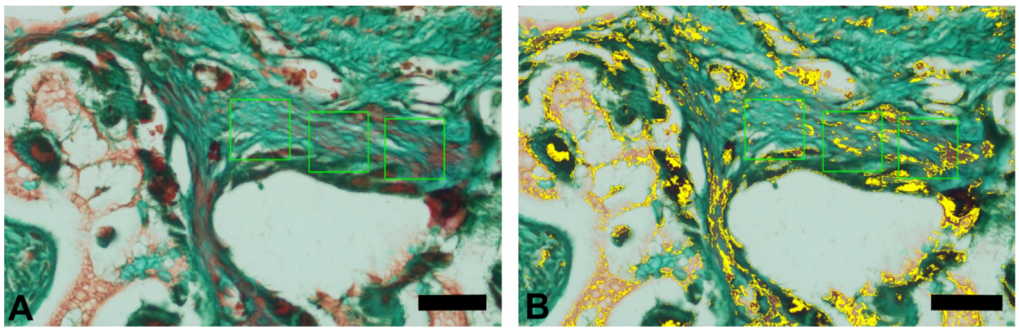

Figure 2. Histomorphometric analysis performed on a Goldner trichrome slide. We can see in the representative scheme performed by GraphPad Prism Version 8.0 (GraphPad, San Diego, CA, USA), the chosen boundary areas (**A**), to measure the percentage of green color representing the newly formed matrix (**B**). Scale bar 100 µm, ×400 magnification.

Masson's trichrome (MT) is a special stain used mainly to characterize and discriminate different tissues, including bone, where, when stained in green or blue, the collagen present in the ossification process is visible. When collagen is stained green, the stain is called Goldner's modified Masson's trichrome. Phosphotungstic or phosphomolybdic acid is used along with anionic dyes to create a balanced color solution. Staining consists of a sequence of staining with iron hematoxylin, which stains the nuclei black; Biebrich scarlet,

which stains the cytoplasm red; and aniline blue or light green aniline, which stains the collagen blue or green, respectively.

2.6.3. Statistical Analysis

The data were analyzed using one-way ANOVA, followed by the Wilcoxon matched pair test ($p < 0.05$). All analyses were performed with specific software (GraphPad Prism Version 8.0 and BioEstat 5.0).

3. Results

3.1. Goldner's Trichromic Staining

Goldner's trichromic staining was chosen due to its ability to clearly distinguish osteoid and mature collagen bone matrix.

The red stained osteoid matrix was more evident in lining the bone marrow, blood vessels and the biomaterials. Group differences relied on the amount of red staining (Figure 3).

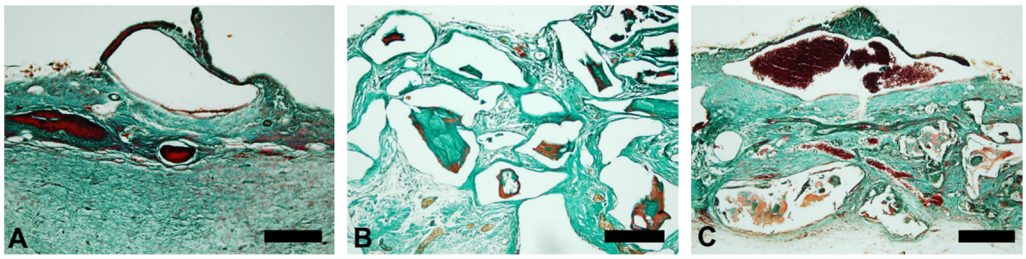

Figure 3. Goldner's trichrome-stained slides photomicrographs showing the representative images of each experimental group that were observed and evaluated. The osteoid bone matrix presents a red color and the bone matrix mature collagen can be observed in green: (**A**) control group (CTRL), (**B**) Bio Oss group (Bioss) and (**C**) Blue Bone group (REG). Scale bar 100 µm, ×200 magnification.

The non-parametric Kruskal–Wallis test showed a very significant statistical relevance in the REG group in relation to the others, showing that the production of a newly formed matrix is more relevant in this group (Figures 4 and 5 and Table 1).

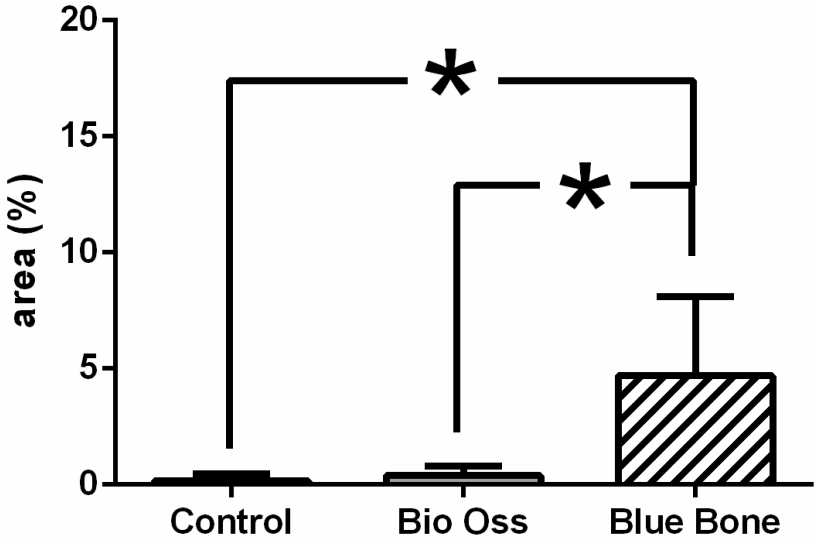

Figure 4. Result of the histomorphometric analysis in the osteoid bone matrix bone areas stained by Goldner's trichrome method: control group (CTRL), Bio Oss group (Bioss) and Blue Bone group (REG). * $p < 0.0001$.

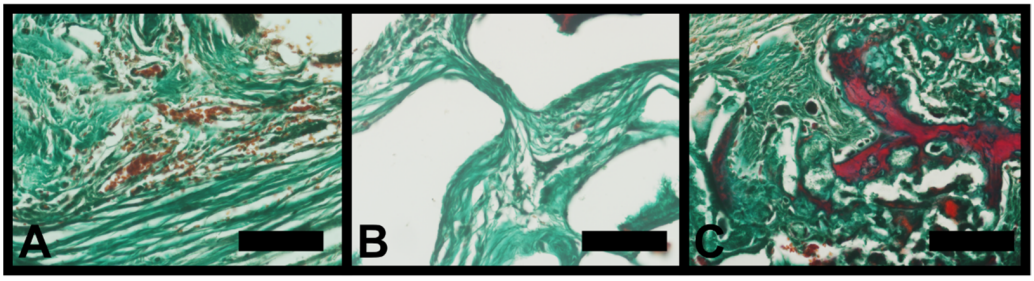

Figure 5. In photomicrography-stained slides with Goldner's trichrome, the red color suggests the formation of the newly formed matrix (osteoid) in the groups; (**A**) control group, (**B**) Bioss group and (**C**) Blue Bone group (REG). Scale bar 100 µm, ×400 magnification.

Table 1. Statistical analysis indicating significance, with *** $p < 0.5$, in relation to the CTRL and Bioss group in comparison with the REG group.

Kruskal–Wallis Test			
Mean	0.516	0.3936	4.685
Std. Deviation	0.314	0.3981	3.405
p value			0.0001
Exact or approximate *p* value?			Exact
p value summary			***

3.2. Osteopontin

Osteopontin-stained slides showed brownish deposits mostly found scattered in the decalcified bone matrix. Some round-nucleus cells (probably osteoblasts) presented high intensity deposits in cytoplasm. These round-nucleus-immunoreactive cells were found in higher numbers around biomaterials groups (Bioss, REG) (Figure 6).

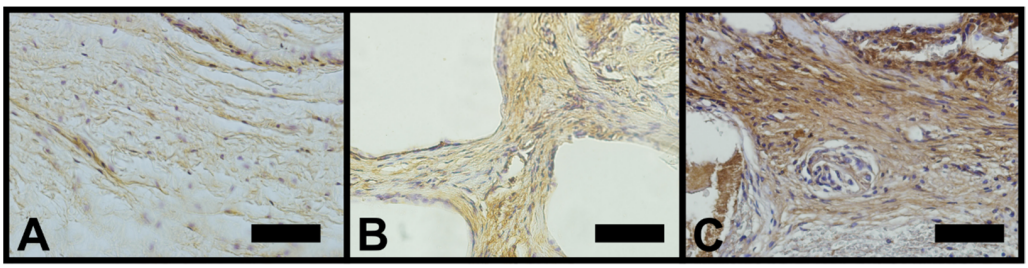

Figure 6. In osteopontin-stained slides photomicrography, shades of brown indicate osteopontin deposits and suggest the activity of cells involved in the bone remodeling process (osteoblasts). (**A**) Control group (CTRL), (**B**) Bio Oss group (Bioss) and (**C**) Blue Bone group (REG) Scale bar 100 µm, ×400 magnification.

The non-parametric Kruskal–Wallis test showed a very significant statistical relevance between the REG and Bioss groups in relation to the CTRL group, showing that there was greater cellularity in the groups with the use of biomaterial than with the use of the clot (Figure 7, Table 2).

3.3. Vascular Endothelial Growth Factor (VEGF)

Vascular endothelial growth factor-immunoreactivity (VEGF-ir) was observed mainly in cells' cytoplasm close to and in the blood vessels in all tested groups. However, in the REG group only, VEGF-ir was found in round nucleus cells scattered around nano-hydroxyapatite/beta-tricalcium phosphate and inside the degrading biomaterial as well (Figure 8).

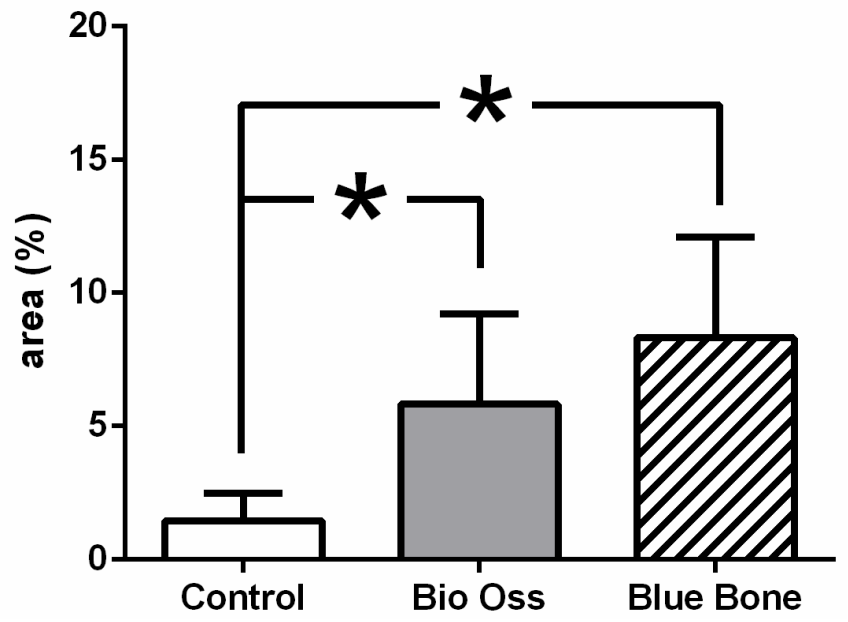

Figure 7. Results of the histomorphometric analysis performed by areas: control group (CTRL), Bio Oss group (Bioss) and Blue Bone group (REG). * $p < 0.0072$.

Table 2. Through the analyzes we can observe a statistical relevance with *** $p < 0.5$ in relation to the REG and Bioss groups compared to the CTRL group.

Kruskal–Wallis Test			
Mean	1.447	5.804	8.279
Std. Deviation	1.024	3.36	3.823
p value			0.0072
Exact or approximate *p* value?			Exact
p value summary			***

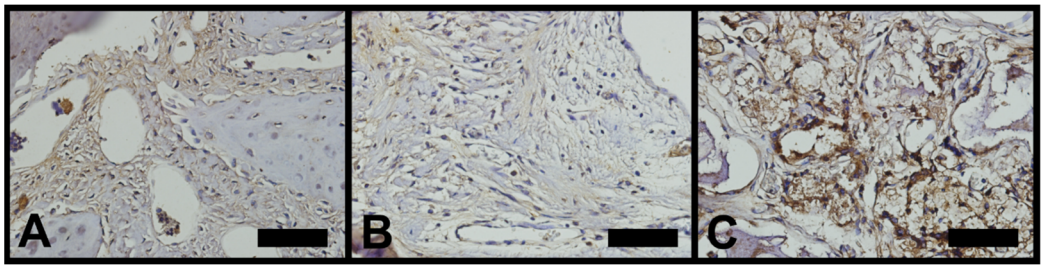

Figure 8. In VEGF-stained photomicrography, the brownish deposits indicate VEGF's presence and its activity, which is involved in the process of the formation of new blood vessels. (**A**) Control group (CTRL), (**B**) Bio Oss group (Bioss) and (**C**) Blue Bone group (REG). Scale bar 100 µm, ×400 magnification.

The non-parametric Kruskal–Wallis test showed that a very significant statistical relevance was found in the REG group in relation to the others, showing an increase in the growth rate of new blood vessels in the REG group (Figure 9, Table 3).

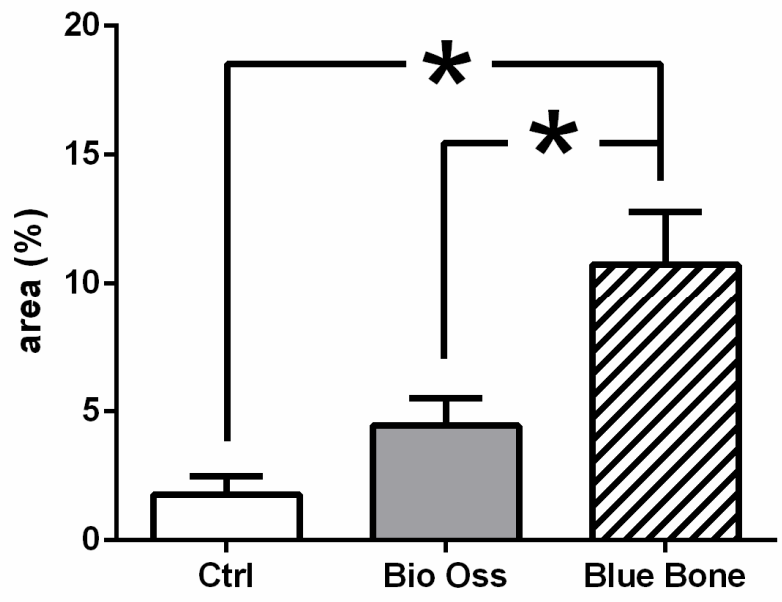

Figure 9. Results of the histomorphometric analysis performed by areas: control group (CTRL), Biooss group (Bioss) and Blue Bone group (REG). * $p < 0.0001$.

Table 3. We can observe through the analyses a statistical relevance with *** $p < 0.5$ in relation to the CTRL and Bioss groups in comparison with the REG group.

Kruskal–Wallis Test			
Mean	1.778	4.439	10.71
Std. Deviation	0.7124	1.049	2.068
p value			0.0001
Exact or approximate *p* value?			Exact
p value summary			***

4. Discussion

In this research model, the nano-hydroxyapatite/beta-tricalcium phosphate compound induced a higher immunoreactivity of osteopontin and VEGF than xenogenic biomaterial and control group in the calvarial critical bone defects model. The same finding was observed in relation to Goldner's trichrome staining. Goldner's trichrome staining is a very appropriate technique to evaluate bone or bone regenerative process. In this staining method, the osteoid bone matrix, which is richer in different types of proteins, is observed in red. On the other hand, the calcified bone matrix, which is richer in type I collagen, is observed in green [14].

Several authors analyzing nano-hydroxyapatite in critical defects have concluded that porous nano-hydroxyapatite scaffolds can promote angiogenesis in the early stage of bone regeneration, suggesting that the graft has significant potential as a bioactive material for bone regeneration in large-scale defects [15–17]. The biochemical mechanism of nano-hydroxyapatite VEGF expression-induction and the subsequent blood vessel enhancing effect was not fully described yet. However, the biomaterial pore size and superficial area seems to have a relevant role. It is believed that a greater area and pore size improve cell adhesion and proliferation, including blood vessels [15]. From this perspective, nano-hydroxyapatite would perform better than xenogenic hydroxyapatite due to its greater surface area and pores size.

Hu J et al. [18] analyzed the morphology response of nano-hydroxyapatite particles in relation to bone formation. They obtained as results that nano-hydroxyapatite favored cell adhesion and promoted osteogenic differentiation, as evidenced by the up-regulated

expression of osteogenic genes, increasing alkaline phosphatase activity and increasing osteopontin production. In the present study, we can observe similar results when comparing the cell adhesion response of micro-hydroxyapatite in relation to nano-hydroxyapatite. Therefore, it is already possible to say that the organized scaffolds provided by nanotechnology favor cell differentiation.

Vascularization is a pivotal and step-limiting process in bone regeneration. Different types of cell modulators and growth factors may contribute to blood vessel sprouting; however, VEGF is the central player. VEGF is more intensely expressed in the first few days of the regenerative process, basically due to local hypoxia. VEGF induces endothelial cell division and capillary sprouting; additionally, it is related to osteogenic cell migration and differentiation [19]. In addition to hydroxyapatite-based biomaterials, functionally modified polyethylene glycol-based hydrogel can successfully induce VEGF gene expression and consequently be considered in bone regenerative therapeutic protocols [20].

In a series of studies, when evaluating the response of new blood vessel formation through the VEGF in critical defects in rat calvaria, it was possible to reach the conclusion that the use of biomaterials from different sources presents more statistically relevant responses than when compared with clot use [21–24]. These results were very important for the elaboration of the methodology of this study, and we can verify that the use of nano-hydroxyapatite and micro-hydroxyapatite obtained similar results to the studies that served as support, in addition to the fact that nano-hydroxyapatite promotes a more adequate response to the protein of signaling the formation of new blood vessels.

Through immunohistochemistry, histology and scanning electronic microscope analysis, the factors involved in bone regeneration processes can be characterized in a broader and easier way [25]. A study that analyzed the use of Masson's trichrome, metaloproteinase (mmp-9), periodic acid Schiff (PAS), tumor necrosis factor (TNF-alpha) and associated ultrastructural results in non-critical defects in rat calvaria compared the use of clots, xenogeneic hydroxyapatite and synthetic nano-hydroxyapatite, reaching the conclusion that nano-hydroxyapatite presented a more favorable inflammatory response, formation of a more relevant bone matrix and it was possible to identify some structures involved in the bone repair process through electron microscopy of sweep [26]. These results corroborate the findings found in this study, even in critical defects, indicating that the use of synthetic nano-hydroxyapatite has become the best alternative for bone defect reconstruction, whether critical or non-critical.

It is noteworthy that this study addressed the bone repair process in only one surgical time of late healing (60 days), indicating a better formation of bone matrix for the nano-hydroxyapatite group; in addition, only two immunohistochemical modulators were used (osteopontin and VEGF), limiting a wide discussion on the healing process and bone remodeling. However, all findings are of great scientific relevance and encourage further investigations on the subject.

5. Conclusions

We can conclude from the results presented in this study that:

a. Synthetic nano-hydroxyapatite had more significant relevance in the formation of newly formed bone matrix compared to xenogeneic hydroxyapatite and clot groups.
b. The rate of the protein that promotes the growth of new blood vessels (VEGF) was higher in the nano-hydroxyapatite group than in the other groups.
c. The response of the extracellular matrix protein (osteopontin) was similar in the synthetic nano-hydroxyapatite and xenogeneic hydroxyapatite groups compared to the control group.

Synthetic nano-hydroxyapatite proved to be a biomaterial with excellent biological response, thus being indicated for any type of bone reconstruction.

Author Contributions: I.S.d.S.: writing the manuscript, I.d.S.B.: sample characterization, co-writing the manuscript. L.F.: SEM analysis, co-writing the manuscript. M.J.d.S.P.: histologyis, animal surgery, histologyis. V.H.V.d.O.: histologyis, immunohistochemistry. A.L.R.N.: immunohistochemistry. J.J.d.C.: animal surgery, co-writing the manuscript. All authors have read and agreed to the published version of the manuscript.

Funding: This research received financial support from the Brazilian agencies CNPq, FAPERJ, CAPES, LUBT, Fisclinex and UERJ.

Conflicts of Interest: The authors declare no conflict of interest.

References

1. Li, N.; Wu, G.; Yao, H.; Tang, R.; Gu, X.; Tu, C. Size effect of nano-hydroxyapatite on proliferation of odontoblast-like MDPC-23 cells. *Dent. Mater. J.* **2019**, *38*, 534–539. [CrossRef]
2. Marycz, K.; Smieszek, A.; Targonska, S.; Walsh, S.A.; Szustakiewicz, K.; Wiglusz, R.J. Three dimensional (3D) printed polylactic acid with nano-hydroxyapatite doped with europium(III) ions (nHAp/PLLA@Eu^{3+}) composite for osteochondral defect regeneration and theranostics. *Mater. Sci. Eng. C Mater. Biol. Appl.* **2020**, *110*, 110634. [CrossRef]
3. Da Silva Brum, I.; de Carvalho, J.J.; da Silva Pires, J.L.; de Carvalho, M.A.A.; Dos Santos, L.B.F.; Elias, C.N. Nanosized hydroxyapatite and β-tricalcium phosphate composite: Physico-chemical, cytotoxicity, morphological properties and in vivo trial. *Sci. Rep.* **2019**, *9*, 19602. [CrossRef]
4. Da Silva Brum, I.; Frigo, L.; Lana Devita, R.; da Silva Pires, J.L.; Hugo Vieira de Oliveira, V.; Rosa Nascimento, A.L.; de Carvalho, J.J. Histomorphometric, Immunohistochemical, Ultrastructural Characterization of a Nano-Hydroxyapatite/Beta-Tricalcium Phosphate Composite and a Bone Xenograft in Sub-Critical Size Bone Defect in Rat Calvaria. *Materials* **2020**, *13*, 4598. [CrossRef]
5. De Oliveira Junior, J.M.; Montagner, P.G.; Carrijo, R.C.; Martinez, E.F. Physical characterization of biphasic bioceramic materials with different granulation sizes and their influence on bone repair and inflammation in rat calvaria. *Sci. Rep.* **2021**, *11*, 4484. [CrossRef]
6. Wang, X.; Li, G.; Guo, J.; Yang, L.; Liu, Y.; Sun, Q.; Li, R.; Yu, W. Hybrid composites of mesenchymal stem cell sheets, hydroxyapatite, and platelet-rich fibrin granules for bone regeneration in a rabbit calvarial critical-size defect model. *Exp. Ther. Med.* **2017**, *13*, 1891–1899. [CrossRef]
7. Brum, I.S.; Elias, C.N.; de Carvalho, J.J.; Pires, J.L.; Pereira, M.J.; de Biasi, R.S. Properties of a bovine collagen type I membrane for guided bone regeneration applications. *e-Polymers* **2021**, *21*, 210–221. [CrossRef]
8. Wang, Z.; Hu, H.; Li, Z.; Weng, Y.; Dai, T.; Zong, C.; Liu, Y.; Liu, B. Sheet of osteoblastic cells combined with platelet-rich fibrin improves the formation of bone in critical-size calvarial defects in rabbits. *Br. J. Oral. Maxillofac. Surg.* **2016**, *54*, 316–321. [CrossRef] [PubMed]
9. Jin, H.; Zhang, K.; Qiao, C.; Yuan, A.; Li, D.; Zhao, L.; Shi, C.; Xu, X.; Ni, S.; Zheng, C.; et al. Efficiently engineered cell sheet using a complex of polyethylenimine-alginate nanocomposites plus bone morphogenetic protein 2 gene to promote new bone formation. *Int. J. Nanomed.* **2014**, *9*, 2179–2190.
10. França, R.; Samani, T.D.; Bayade, G.; Yahia, L.; Sacher, E. Nanoscale surface characterization of biphasic calcium phosphate, with comparisons to calcium hydroxyapatite and β-tricalcium phosphate bioceramics. *J. Colloid Interface Sci.* **2014**, *420*, 182–188. [CrossRef] [PubMed]
11. Dey, R.E.; Wimpenny, I.; Gough, J.E.; Watts, D.C.; Budd, P.M. Poly (vinylphosphonic acid-co-acrylic acid) hydrogels: The effect of copolymer composition on osteoblast adhesion and proliferation. *J. Biomed. Mater. Res. A* **2018**, *106*, 255–264. [CrossRef]
12. Joshi, S.; Mahadevan, G.; Verma, S.; Valiyaveettil, S. Bioinspired adenine-dopamine immobilized polymer hydrogel adhesives for tissue engineering. *Chem. Commun. (Camb.)* **2020**, *56*, 11303–11306. [CrossRef]
13. Lee, J.H.; Ryu, M.Y.; Baek, H.R.; Lee, K.M.; Seo, J.H.; Lee, H.K. Fabrication and evaluation of porous beta-tricalcium phosphate/hydroxyapatite (60/40) composite as a bone graft extender using rat calvarial bone defect model. *Sci. World J.* **2013**, *2013*, 481789. [CrossRef]
14. Gruber, H.E. Adaptations of Goldner's Masson trichrome stain for the study of undecalcified plastic embedded bone. *Biotech. Histochem.* **1992**, *67*, 30–34. [CrossRef]
15. Du, B.; Liu, W.; Deng, Y.; Li, S.; Liu, X.; Gao, Y.; Zhou, L. Angiogenesis and bone regeneration of porous nano-hydroxyapatite/coralline blocks coated with rhVEGF165 in critical-size alveolar bone defects in vivo. *Int. J. Nanomed.* **2015**, *10*, 2555–2565. [CrossRef]
16. Dreyer, C.H.; Kjaergaard, K.; Ding, M.; Qin, L. Vascular endothelial growth factor for in vivo bone formation: A systematic review. *J. Orthop. Translat.* **2020**, *24*, 46–57. [CrossRef]
17. Lytkina, D.; Gutsalova, A.; Fedorishin, D.; Korotchenko, N.; Akhmedzhanov, R.; Kozik, V.; Kurzina, I. Synthesis and Properties of Zinc-Modified Hydroxyapatite. *J. Funct. Biomater.* **2020**, *11*, 10. [CrossRef]
18. Hu, J.; Yang, Z.; Zhou, Y.; Liu, Y.; Li, K.; Lu, H. Porous biphasic calcium phosphate ceramics coated with nano-hydroxyapatite and seeded with mesenchymal stem cells for reconstruction of radius segmental defects in rabbits. *J. Mater. Sci. Mater. Med.* **2015**, *26*, 257. [CrossRef] [PubMed]

19. De Witte, T.M.; Fratila-Apachitei, L.E.; Zadpoor, A.A.; Peppas, N.A. Bone tissue engineering via growth factor delivery: From scaffolds to complex matrices. *Regen. Biomater.* **2018**, *5*, 197–211. [CrossRef]
20. Gaihre, B.; Liu, X.; Li, L.; Lee Miller Ii, A.; Camilleri, E.T.; Li, Y.; Waletzki, B.; Lu, L. Bifunctional hydrogel for potential vascularized bone tissue regeneration. *Mater. Sci. Eng. C Mater. Biol. Appl.* **2021**, *124*, 112075. [CrossRef] [PubMed]
21. Pires, J.L.D.S.; de Carvalho, J.J.; Pereira, M.J.D.S.; Brum, I.D.S.; Nascimento, A.L.R.; Dos Santos, P.G.P.; Frigo, L.; Fischer, R.G. Repair of Critical Size Bone Defects Using Synthetic Hydroxyapatite or Xenograft with or without the Bone Marrow Mononuclear Fraction: A Histomorphometric and Immunohistochemical Study in Rat Calvaria. *Materials* **2021**, *26*, 2854. [CrossRef]
22. Adams, B.R.; Mostafa, A.; Schwartz, Z.; Boyan, B.D. Osteoblast response to nanocrystalline calcium hydroxyapatite depends on carbonate content. *J. Biomed. Mater. Res. A* **2014**, *102*, 3237–3242. [CrossRef] [PubMed]
23. Harada, S.; Nagy, J.A.; Sullivan, K.A.; Thomas, K.A.; Endo, N.; Rodan, G.A.; Rodan, S.B. Induction of vascular endothelial growth factor expression by prostaglandin E2 and E1 in osteoblasts. *J. Clin. Investig.* **1994**, *93*, 2490–2496. [CrossRef]
24. Liu, W.; Du, B.; Tan, S.; Wang, Q.; Li, Y.; Zhou, L. Vertical Guided Bone Regeneration in the Rabbit Calvarium Using Porous Nanohydroxyapatite Block Grafts Coated with rhVEGF$_{165}$ and Cortical Perforation. *Int. J. Nanomed.* **2020**, *15*, 10059–10073. [CrossRef] [PubMed]
25. Gao, J.; Huang, J.; Shi, R.; Wei, J.; Lei, X.; Dou, Y.; Li, Y.; Zuo, Y.; Li, J. Loading and Releasing Behavior of Selenium and Doxorubicin Hydrochloride in Hydroxyapatite with Different Morphologies. *ACS Omega* **2021**, *6*, 8365–8375. [CrossRef] [PubMed]
26. Da Silva Brum, I.; Frigo, L.; Goncalo Pinto Dos Santos, P.; Nelson Elias, C.; da Fonseca, G.A.M.D.; Jose de Carvalho, J. Performance of Nano-Hydroxyapatite/Beta-Tricalcium Phosphate and Xenogenic Hydroxyapatite on Bone Regeneration in Rat Calvarial Defects: Histomorphometric, Immunohistochemical and Ultrastructural Analysis. *Int. J. Nanomed.* **2021**, *16*, 3473–3485. [CrossRef] [PubMed]